Propagation of Degenerate Band-Edge Modes Using Dual Nonidentical Coupled Transmission Lines

A. Muhammed Zuboraj, B. Kubilay Sertel, and C. John L. Volakis

Phys. Rev. Applied **7**, 064030 — Published 28 June 2017

DOI: 10.1103/PhysRevApplied.7.064030

Propagation Model of Degenerate Band Edge Modes Using Dual Non-identical Pair of Coupled Transmission Lines

A. Muhammed Zuboraj,* B. Kubilay Sertel,† and C. John L. Volakis‡
ElectroScience Laboratory, Department of Electrical and Computer Engineering
The Ohio State University, Columbus, OH, 43212, USA.

Degenerate Band Edge (DBE) modes are known for their exceptionally high field intensity at near flat dispersion diagram profile. Due to the latter property, resonances supported by these modes are associated with very strong field at the band edge. DBE and similar resonances of this class have been typically realized by introducing anisotropic dielectric slabs in volumetric photonic crystals. By contrast, in this paper, we present an analytic model of DBE modes using a simple set of non-identical coupled transmission lines. The unequal phase velocities of the supported waves supported by these transmission lines lead to mode degeneracy, that in turn provide quartic solutions of dispersion ($\omega - \beta$) relations. DBE mode appear as one these quartic solutions. As such, the proposed model generalizes the concept of DBE modes using the construct of non-identical coupled transmission lines. In this paper, we also propose a propagation medium using a dual pair of non-identical transmission lines. The medium is referred to as 'butterfly' structure and is composed of four coupled transmission lines. These four coupled transmission lines generate $TM_{01}-$like Degenerate Band Edge mode. This is done by coupling the TE modes supported on each pair of the transmission lines. Mode purity at the resonance frequency and the intense field profile on the axis are properties that can be exploited for high power microwave sources.

Keywords: Degenerate Band Edge, Coupled Transmission Lines

I. INTRODUCTION

Periodic and/or metamaterial structures are routinely used to control propagation characteristics of electromagnetic waves. They have been successfully used in numerous applications, including antenna arrays [1], leaky wave antennas [2], electromagnetic bandgap structures [3], artificial magnetic conductors [4], frequency selective surfaces [5] and slow wave realization [6–8]. Depending on the unit elements used in periodic layers, different properties of electromagnetic wave propagation is achieved. For example, (i) using split rings and copper strips in a two dimensional periodic array, negative index of refraction was achieved [9]; (ii) periodically spaced antenna elements provide arbitrary beam-forming for multipath signal reception and target tracking [10, 11]; (iii) two dimensional textured lattice of resonant elements in metal sheet forms high impedance surface, preventing certain frequencies from propagation [4]. However, the simplest form of periodic structures is periodic dielectric stacks that have been traditionally used to achieve electromagnetic bandgaps [12]. In this paper, we focus on the latter and propose a replacement of those dielectrics using coupled transmission lines.

Periodic stacks of dielectrics are often referred to as photonic crystals as in Fig. 1(a). These crystals support band gaps in their dispersion diagrams caused by the coupling of forward and backward waves. The actual dispersion curve can be of second order with the edge of the bandgap located at the $\beta p = \pi$ point, referred to as 'regular band edge (RBE)' (Fig. 1(a)). Field intensity is typically high at the band edge and is proportional to N^2 [13], where N is the number of periodic cells in an array.

When anisotropic dielectric layers are used to form unit cells of the stack, additional resonances can be supported [7, 14, 15]. The dispersion diagram for these cases can be up to fourth order and the edge of the band is usually referred to as Degenerate Band Edge (DBE) [15, 16]. Due to this fourth order $\omega - \beta$ relation, the field intensity at the band edge is proportional to N^4 [13, 15], where N is the number of periodic cells in an array. That is, huge field enhancement is associated with this resonance realized by these special DBE crystals[13, 15]. This property has been exploited in the past to improve the directivity of dipole antennas [17]. The insertion of a magnetic layer into the unit cell can generate Magnetic Photonic Crystal modes [8, 18]. These modes are specially useful to achieve frequency independent scanning of leaky wave antennas [2].

Despite their attractive properties and applications, DBE crystals lack simplicity in realization. These crystals are usually formed of bulk dielectric slabs and require large space. Due to this, the DBE crystals are difficult to conform into certain applications e.g. electronic chips, planner antennas, waveguides etc. where space is limited. Therefore, alternate approaches to realize such media are of interest. As shown in [13, 19, 20], the physics of DBE/MPC modes are associated with anisotropic media and special mode coupling mechanism. Already, as a simpler alternative, Locker et. al. [7] introduced the concept of coupled transmission lines (TLs) to emulate photonic crystals. As shown by Locker et. al. [7], coupled and un-

* zuboraj.1@buckeyemail.osu.edu
† sertel.1@osu.edu
‡ volakis.1@osu.edu

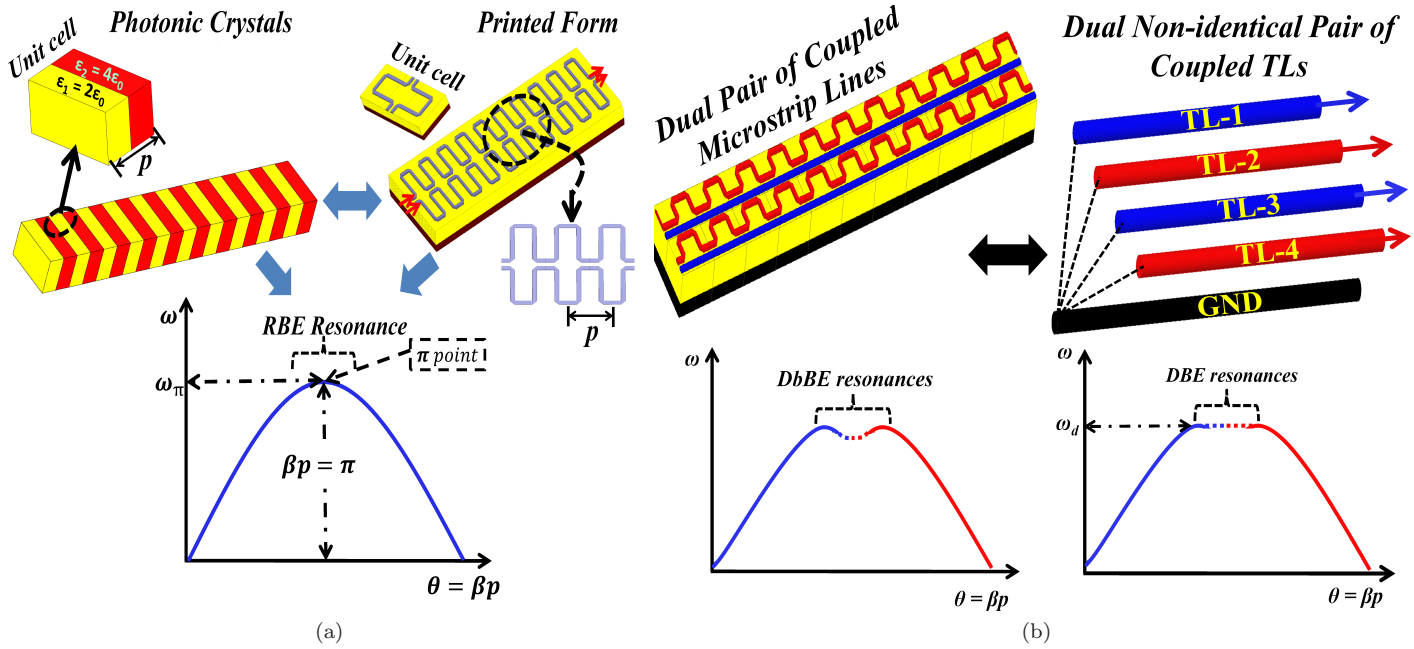

FIG. 1. (a) 1-D photonic crystals composed of dielectric stacks (top left); Equivalent medium in the form of printed circuits (top right); $\omega - \beta$ diagram showing regular band edge resonance (bottom) (b) Dual pair of coupled non-identical microstrip lines and its equivalent circuit; DbBE (bottom left) and DBE (bottom right) resonances are supported on these lines.

coupled sections of meandered microstrip lines emulate the required anisotropy for the realization of DBE modes. This approach has also been used to realize miniaturized antennas [6] and to achieve frequency independent beams-scanning [2] in leaky wave antennas.

Although the concept of coupled TLs has been successfully used [21] in various applications, its potential has yet to be exploited. For example, DBE modes have yet to be realized inside waveguide structures. Recently, Othman et al. [22] proposed a medium formed by misaligned elliptic irises that demonstrates DBE modes inside circular waveguides. These modes can be useful to amplify RF wave that interacts with an electron beam [23] in traveling wave tubes and/or Backward Wave Oscillators (BWOs). Typically, the electronic efficiency of traveling wave tubes and BWOs is low and dependent on the axial field intensity of the waveguide modes. Therefore, the introduction of new modes within waveguide that support strong axial electric field at the center can improve beam-to-RF mode interactions. However, the elliptic irises [22] do not support pure TM_{01} modes, an essential property for efficient beam-wave interactions. Even though, the DBE mode was demonstrated in dispersion diagrams [22], the physics of mode coupling in the presence of natural TE and TM modes inside has not been explained. To do so, a generalized approach of mode coupling mechanism is introduced in this paper.

We present a generalized method of mode coupling using non-identical coupled transmission lines to realize fourth-order dispersion diagrams (DBE modes). In previous papers [7, 8], only a single pair of coupled TLs was considered and the associated coupled modes were TEM types. However, single pair of non-identical TLs does not provide sufficient coupling to support DBE modes due to the presence of the natural waveguide (TE, TM) modes in background. Also, in previous works, the coupling was not characterized in terms of simple (L, C) parameters. Further, as noted above, the mode coupling mechanisms leading to higher-order dispersion was not explained.

In this paper, we build upon the concept of coupled transmission lines and proceed to generate higher-order dispersion curves using a new 'coupled mode' technique for dual pairs of non-identical coupled TLs (Fig. 1(b)). The key characteristics of the new coupled TLs are:

1. Non-identical TLs
2. Coupled (L, C) parameters
3. Coupling co-efficients, later defined as K_{c1}, K_{c2}, and K_{c3};

These will be explained in Section-II. Section-III presents a 'butterfly' structure that realizes the non-identical TLs. The structure demonstrates DBE modes with $TM_{01}-$like field profile. In section-IV, a BWO example will be given as a sample of vacuum tube applications using four coupled transmission lines. It is shown that, the field enhancement due to DBE mode improves the BWO's electronic efficiency. Overall, we believe that the findings and analysis in this paper will provide a basis for dispersion engineering pertaining to other applications such as resonator antennas [24], waveguides [25] and cavities [26].

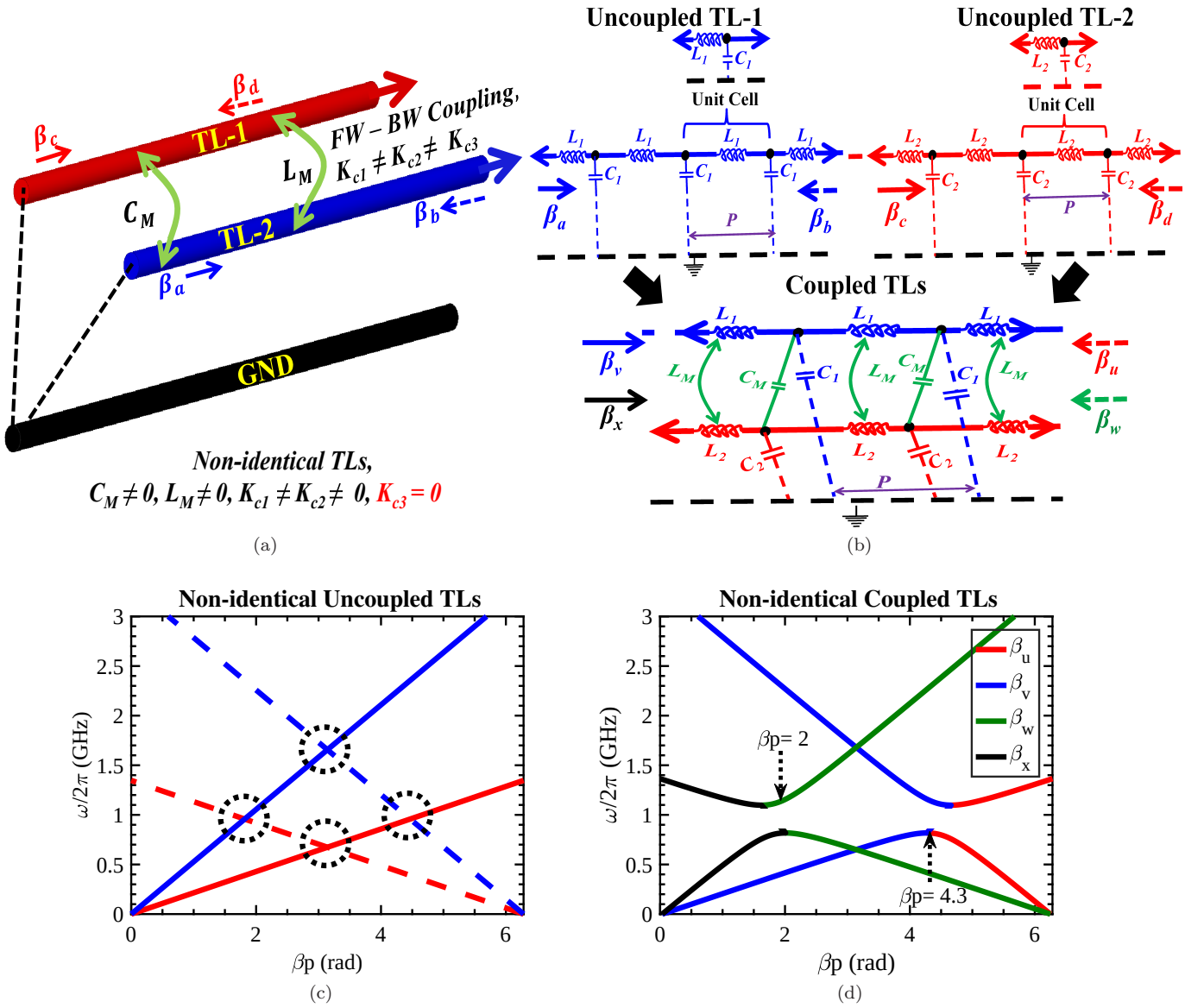

FIG. 2. (a) A pair of coupled non-identical TLs to realize DbBE and DBE modes. Two oppositely traveling waves with unequal phase velocities couple through mutual inductance, L_M and capacitance, C_M (b) Pair of uncoupled and coupled non-identical TLs supporting forward and backward waves whose propagation constants are defined in (2)-(9). (c) $\omega - \beta$ dispersion diagram of the uncoupled TLs for each of the supported modes given in (2)-(5). The solid blue and red line represent (2) and (4), while dashed blue and red lines represent (3) and (5). (d) Regular band edge resonances realized by the non-identical coupled TLs are found due to unequal velocities (v_1, v_2) (6)-(9). These curves refer to circuit parameters $(L_1, C_1) \equiv$(16.17 μH, 68.8 pF) and $(L_2, C_2) \equiv$(6.5 μH, 27.52 pF).

II. DISPERSION ENGINEERING USING DUAL NON-IDENTICAL PAIR OF TLS

A. Background

Transmission lines are inherently periodic structures as they can be modeled with periodically spaced lumped elements (L, C) of period p. TLs support both forward and backward waves. By controlling the (L, C) parameters of the TLs, slow waves $(v \ll c)$ can be realized. Indeed, this property has been used to enhance coupling of the electron beam to RF waves in traveling wave tubes and BWO applications. Examples of coupled transmission lines include double helix [27], ring-bar [28, 29] and ring-loop [30] etc. For these cases, the TL pair had identical lumped elements (L, C) and supports regular band edge mode only. This mode is observed at the frequency (ω_π) corresponding to $\beta p = \pi, 3\pi, 5\pi, ...$ in the dispersion diagram, where β is the propagation constant and ω_π is the angular frequency. We remark that regular band edge

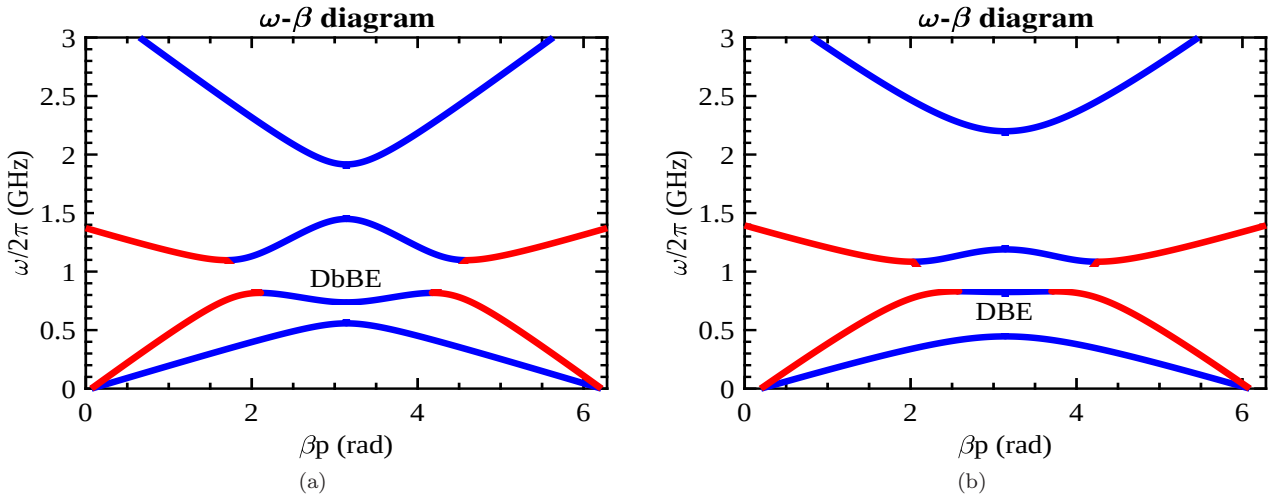

FIG. 3. $\omega - \beta$ diagrams associated with coupled pairs of TLs. The (L, C) parameters of the coupled TLs of each pair are: $(L_1, C_1) \equiv$(16.17 μH, 68.8 pF) and $(L_2, C_2) \equiv$(6.5 μH, 27.52 pF). (a) DbBE dispersion curves viz. weak coupling of the dual TL pair. For DbBE mode, the coupling parameters are: $K_{c1} = K_{c2} = K_{c3} = 20.85$ (b) DBE dispersion curves viz. strong coupling of the dual TL pair. These are fourth-order curves and higher-order dispersion condition: $\frac{\partial^3 \omega}{\partial \beta^3} \neq 0.$, the coupling parameters are: $K_{c1} = K_{c2} = 20.85 \neq 50 = K_{c3}$

resonances are a consequence of the coupling between the forward and backward wave modes [29, 31, 32].

When the coupled TLs are not identical viz. composed of different lumped elements (blue and red) as shown in Fig. 1(b) (top), the forward and backward waves have unequal phase and group velocities and give rise to double band edge (DbBE) as in Fig. 1(b) (bottom left). The term 'double band' originates from the presence of dual RBE resonances in the dispersion diagram. Typically, DbBE resonances are weak in comparison to DBE resonances and are not useful since the field intensity at the band edge is proportional to N^2. The non-identical nature of the TLs induces weak coupling between two RBE resonances, creating a crest in between them (Fig. 1(b)). The latter affects the electric field intensity at the band edge. The coupling strength between these two RBE resonances is completely dependent on the type of mode involved i.e. the field profiles of each mode.

In contrast, DBE modes are quite strong due to their degeneracy at the band edge. The coupling strength between the TLs, if chosen appropriately by modifying the geometry of RF structure, furnish appropriate coupling environment required for DbBE modes to evolve into DBE modes (Fig. 1(b) (bottom right)). Therefore, DBE resonance can be achieved if the lumped parameters of the non-identical coupled TLs are chosen appropriately. Unlike DbBE resonances, four modes are strongly coupled together to form DBE resonances. Due to this, field intensity at the band edge is couple of degrees higher as compared to RBE or DbBE resonances. Actually, more than second-order dispersion can be achieved using a pair of non-identical coupled TLs. Depending on the modes involved in the coupling process and lumped (L, C) elements, DbBE or DBE modes can be achieved. Below, we provide a theoretical analysis for the coupled TLs to generate higher-order dispersion curves.

B. Theoretical Analysis

The presented analysis follow the coupled mode theory [31, 33]. For any continuously coupled system, the coupled mode propagation constants are functions of the propagation constants of each uncoupled mode [31]. For detailed information about the continuous coupling in periodic systems and the associated propagation constants, please refer to the derivation in the Supplemental material [34]. Since coupled TLs comprise of periodically spaced lumped coupling elements (L_M, C_M), the analogy of continuously coupled system can be translated to coupled transmission line systems. Accordingly, the coupled pair of TLs are associated with the propagation constants [31]:

$$\beta_{\pm} = \frac{\beta_m + \beta_n}{2} \pm \sqrt{(\frac{\beta_m - \beta_n}{2})^2 - K_c^2} \qquad (1)$$

Here, $\beta_m = \omega\sqrt{LC}$, $\beta_n = \frac{2\pi}{p} - \omega\sqrt{LC}$, the uncoupled propagation constants of each line being coupled and $\beta_{\pm}$ refer to the forward and backward modes for the coupled TLs system. Also, the coefficient, K_c represents the coupling between the β_{mn} modes. We remark that (1) is the building block of our analysis. Specifically, by choosing appropriate modes to replace the (β_m, β_n) pair, fourth-order dispersion curves can be generated.

To begin, let us consider two uncoupled TLs associated with different lumped inductances and capacitances (L_1, C_1) and (L_2, C_2). These lines are depicted in blue

and red color in Fig. 2(a), 2(b). Each TL supports forward and backward waves associated with unequal velocities, $\upsilon_1 = \frac{1}{\sqrt{L_1C_1}} \neq \frac{1}{\sqrt{L_2C_2}} = \upsilon_2$. The propagating constants of these four waves are:

$$\beta_a = \omega\sqrt{L_1C_1} = \frac{\omega}{\upsilon_1} \tag{2}$$

$$\beta_b = \frac{2\pi}{p} - \omega\sqrt{L_1C_1} = \frac{2\pi}{p} - \frac{\omega}{\upsilon_1} \tag{3}$$

$$\beta_c = \omega\sqrt{L_2C_2} = \frac{\omega}{\upsilon_2} \tag{4}$$

$$\beta_d = \frac{2\pi}{p} - \omega\sqrt{L_2C_2} = \frac{2\pi}{p} - \frac{\omega}{\upsilon_2} \tag{5}$$

Each of the above β's, gives rise to the linear dispersion curves (2)-(5) in Fig. 2(c). Notably, unlike identical TLs, each line supports non-overlapping forward wave and backward wave modes represented by solid and dashed lines, respectively. We denote the forward wave propagation constants as β_a (solid blue line) and β_c (solid red line). Similarly, β_b (dashed blue line) and β_d (dashed red line) represent the backward wave propagation constants.

When the TLs are coupled, they couple through the forward and backward mode pairs. This gives rise to second-order dispersion curves as in Fig. 2(d). Specifically, the coupling between forward and backward mode pairs e.g. $\beta_a(\omega)$, $\beta_d(\omega)$ and $\beta_b(\omega)$, $\beta_c(\omega)$ gives rise to second-order dispersion curves. The associated propagation constants are given by

$$\beta_u = \frac{\pi}{p} - \frac{\omega}{2}\left(\frac{1}{\upsilon_2} - \frac{1}{\upsilon_1}\right) + \sqrt{\left\{\frac{\pi}{p} - \frac{\omega}{2}\left(\frac{1}{\upsilon_2} + \frac{1}{\upsilon_1}\right)\right\}^2 - K_{c1}^2} \tag{6}$$

$$\beta_v = \frac{\pi}{p} - \frac{\omega}{2}\left(\frac{1}{\upsilon_2} - \frac{1}{\upsilon_1}\right) - \sqrt{\left\{\frac{\pi}{p} - \frac{\omega}{2}\left(\frac{1}{\upsilon_2} + \frac{1}{\upsilon_1}\right)\right\}^2 - K_{c1}^2} \tag{7}$$

$$\beta_w = \frac{\pi}{p} + \frac{\omega}{2}\left(\frac{1}{\upsilon_2} - \frac{1}{\upsilon_1}\right) + \sqrt{\left\{\frac{\pi}{p} - \frac{\omega}{2}\left(\frac{1}{\upsilon_2} + \frac{1}{\upsilon_1}\right)\right\}^2 - K_{c2}^2} \tag{8}$$

$$\beta_x = \frac{\pi}{p} + \frac{\omega}{2}\left(\frac{1}{\upsilon_2} - \frac{1}{\upsilon_1}\right) + \sqrt{\left\{\frac{\pi}{p} - \frac{\omega}{2}\left(\frac{1}{\upsilon_2} + \frac{1}{\upsilon_1}\right)\right\}^2 - K_{c2}^2} \tag{9}$$

It is noted that (6)-(9) represent second-order dispersion curves and are associated with an regular band edge resonances at $\beta p = 2$ (rad) and $\beta p = 4.3$ (rad), respectively. Their associated dispersion curves are given in Fig. 2(d).

To characterize and observe higher-order coupling, we introduce a new coupling parameter, K_{c3}. This quantity represents coupling between β_v and β_w. Since β_v and β_w have same phase velocity at the $\pi-$ point, these pairs couple further inside waveguide and form fourth-order dispersion curves.

$$\beta_1 = \frac{\pi}{p} + \sqrt{\left[\frac{\omega}{2}\left(\frac{1}{\upsilon_1} - \frac{1}{\upsilon_2}\right) - \sqrt{\left\{\frac{\pi}{p} - \frac{\omega}{2}\left(\frac{1}{\upsilon_1} + \frac{1}{\upsilon_2}\right)\right\}^2 - K_{c1}^2}\right] - K_{c3}^2} \tag{10}$$

$$\beta_2 = \frac{\pi}{p} - \sqrt{\left[\frac{\omega}{2}\left(\frac{1}{\upsilon_1} - \frac{1}{\upsilon_2}\right) - \sqrt{\left\{\frac{\pi}{p} - \frac{\omega}{2}\left(\frac{1}{\upsilon_1} + \frac{1}{\upsilon_2}\right)\right\}^2 - K_{c1}^2}\right] - K_{c3}^2} \tag{11}$$

$$\beta_3 = \frac{\pi}{p} + \sqrt{\left[\frac{\omega}{2}\left(\frac{1}{\upsilon_1} - \frac{1}{\upsilon_2}\right) - \sqrt{\left\{\frac{\pi}{p} - \frac{\omega}{2}\left(\frac{1}{\upsilon_1} + \frac{1}{\upsilon_2}\right)\right\}^2 - K_{c2}^2}\right] - K_{c3}^2} \tag{12}$$

$$\beta_4 = \frac{\pi}{p} - \sqrt{\left[\frac{\omega}{2}\left(\frac{1}{\upsilon_1} - \frac{1}{\upsilon_2}\right) - \sqrt{\left\{\frac{\pi}{p} - \frac{\omega}{2}\left(\frac{1}{\upsilon_1} + \frac{1}{\upsilon_2}\right)\right\}^2 - K_{2}^2}\right] - K_{c3}^2} \tag{13}$$

The corresponding propagation constants, β_2 and β_3 are of fourth-order and can be derived using the process described in [31].

When (10)-(13) are plotted in Fig. 3, DbBE and DBE modes are observed subject to appropriate choices for K_{c1}, K_{c2} and K_{c3}. That is, K_{c3} is important in realizing higher-order dispersion curves.

Above, K_{c1}, K_{c2} and K_{c3} signify different mode formation mechanisms. It is noted that these parameters are strongly dependent on geometric features and mode profile. For example, the parameters K_{c1} and K_{c2} represent natural coupling between the forward and backward modes of two non-identical TLs. Each forward and backward wave velocities can be non-identical to each other and degree of coupling is strongly dependent on their field profile.

On the contrary, K_{c3} represents coupling between two RBE resonances of two different modes. Therefore, the derivation of K_{c3} is a cumbersome process and is beyond the scope of this paper. Indeed, a numerical approach can be employed to compute K_{c3}.

We note that special choices for K_{c1}, K_{c2} and K_{c3} lead to the realization of DbBE (Fig. 3(a)) and DBE modes (Fig. 3(b)). For example, a strong flat top fourth-order resonance (DBE mode) is observed for $K_{c1} = K_{c2} \neq K_{c3}$ (Fig. 3(b)). Since the $\omega - \beta$ diagram is a fourth order polynomial, i.e. $\omega \propto (\beta^4)$, the first, second and third derivatives of ω are non-zero at the band edge. This is an important property that verifies the presence of the DBE modes in the dispersion diagram. Recently, Othaman et al. [23] demonstrated that DBE modes can be realized by imposing angular anisotropy using elliptic irises in circular waveguide. In the following section, we present an example of such DBE mode realization using coupled TLs.

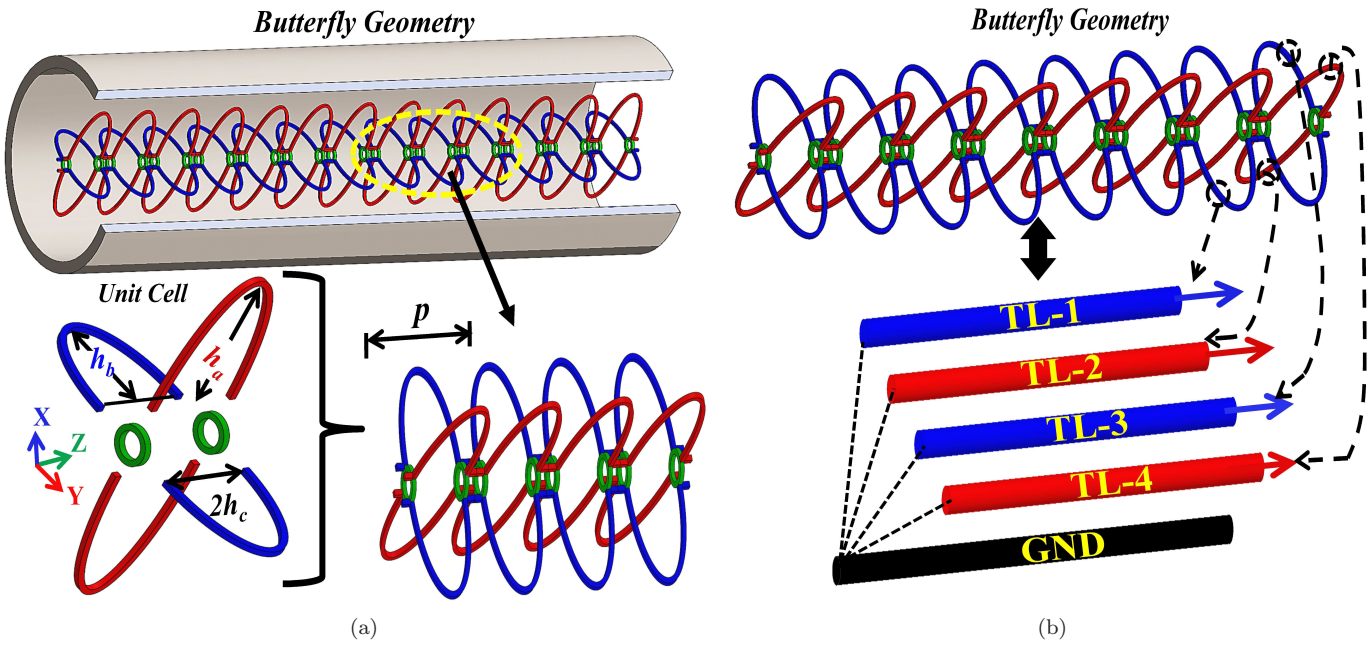

FIG. 4. (a) The 'butterfly' slow wave structure placed within a circular waveguide for realizing DBE modes. Unit cell is shown below the circular waveguide. Each of the four TLs is formed of a series of elliptical loops. Also, a ring at the center of the TLs serve to achieve coupling among the TLs. The dimensions of the elliptical and circular rings are: $h_a = 50.8$ mm, $h_b = 36.4$ mm, $h_c = 7.4$ mm, $p = 22$ mm, r_b = ring radius = 4.5 mm, r_g = waveguide radius = 63.5 mm. Notably, the unequal pairs in different planes emulate non-identical coupled TLs. (b) 'butterfly' geometry and its equivalent TL structure.

III. REALIZATION OF DBE MODE USING 'BUTTERFLY' GEOMETRY

Above, we proposed a pair of non-identical TLs to realize higher-order dispersion curves. However, depending on the geometry and mode profile, the coupling parameters are affected and either DbBE or DBE mode is observed. In this section, we present an example of RF structure based on coupled TLs placed inside a waveguide. As already stated, strong coupling among the non-identical coupled TLs is necessary to achieve DBE modes. Othman et. al. [22] demonstrated such a medium by using misaligned elliptic irises placed on the axis of a circular waveguide.

In this paper, we realized DBE modes using two pairs of free standing wire TLs placed orthogonally to each other. One such structure is demonstrated in Fig. 4(a). The associated structure is formed by a 'butterfly' unit cell. This unit cell is composed of two non-identical pairs of TLs represented by elliptic wires/bars, marked as blue and red in Fig. 4(b). Notably, the four TLs are placed circularly among a set of rings. These rings serve to realize coupling among the four TLs. Each pair of TLs (blue or red) are in essence Curved Ring-bars [29]. The coefficients, K_{c1} and K_{c2} represent the coupling between oppositely traveling modes for the TL pairs. They are given as follows [29]:

$$K_{c1} = \frac{(1+\frac{\pi h_a}{4a})}{E_1(m)}\sqrt{\frac{\beta_a\beta_d}{|\beta_a-\beta_d|}} \tag{14a}$$

$$K_{c2} = \frac{(1+\frac{\pi h_b}{4a})}{E_2(m)}\sqrt{\frac{\beta_b\beta_c}{|\beta_b-\beta_c|}} \tag{14b}$$

where, $E_1(m = \frac{h_a}{h_c}) = \int_0^{\pi/2}\sqrt{1-(m^2-1)\sin^2(\theta)}d\theta$ and $E_2(m = \frac{h_b}{h_c}) = \int_0^{\pi/2}\sqrt{1-(m^2-1)\sin^2(\theta)}d\theta$ is the elliptic integral of the second kind.

In Fig. 4(a), the coupling rings are marked with green color and allow control of mutual inductances/capacitances between the TL pairs. It is noted that each identical pair (blue or red) in Fig. 4 serves as a single TL component of the non-identical TL model as shown in Fig. 2(b). This coupling mechanism serves to:

1. Provide a medium that support slow waves.
2. Lower the cut-off frequency of waveguide modes
3. Facilitates coupling of the lower order modes to form higher-order such as DBE mode.

To illustrate the above mechanism, we refer to Fig. 5(a), 5(b). Indeed, the introduction of 'butterfly' geometry lowered the cut-off frequency of each mode forming slow waves inside the circular waveguide as shown in

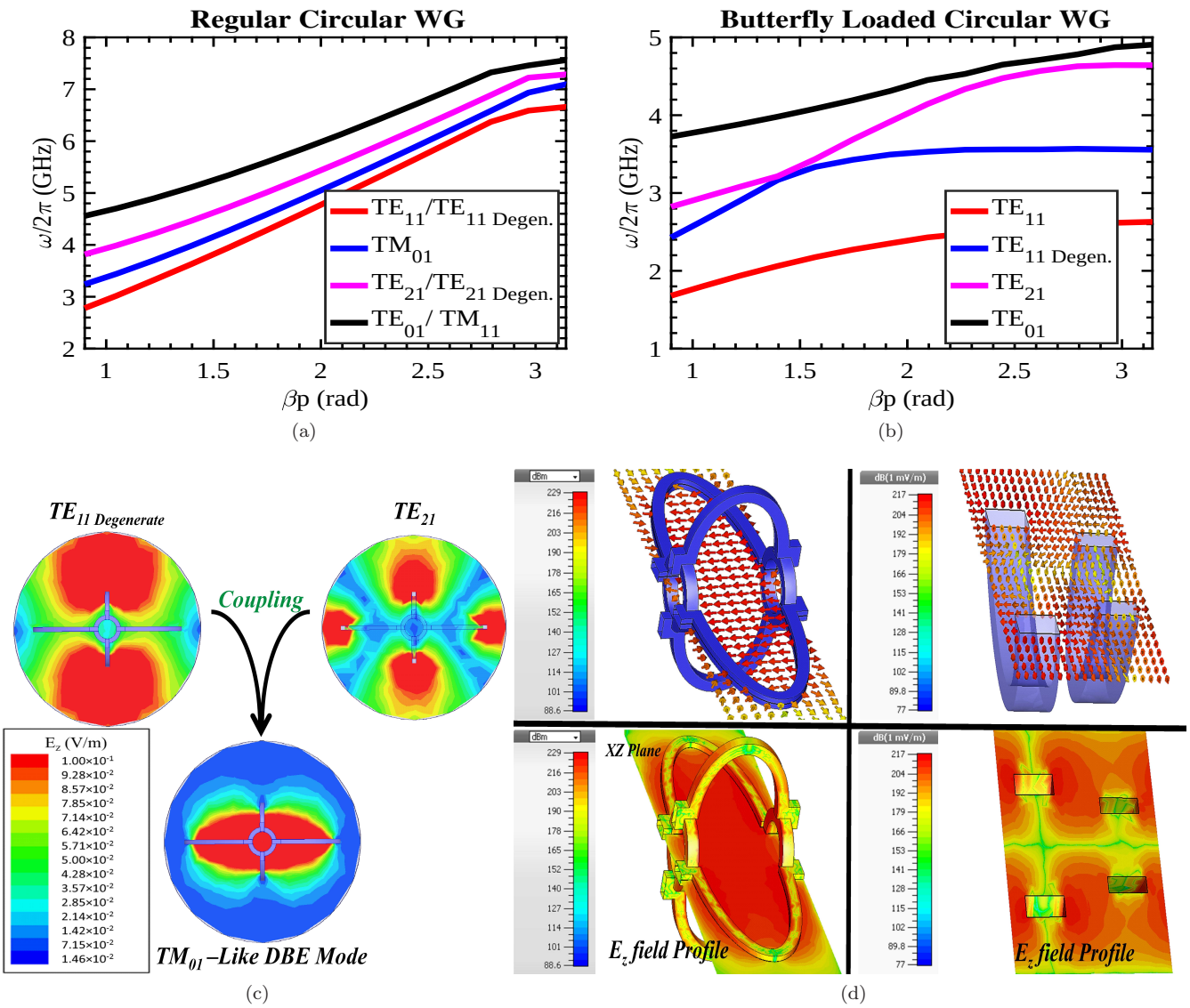

FIG. 5. Comparison of the dispersion diagrams with (a) and without (b) the 'butterfly' periodic geometry inside the circular waveguide. As seen, the introduction of the 'butterfly' TL structure lowered the cut-off frequency of each mode by splitting the TE_{11} degenerate modes. (c) Illustration of coupling to form the DBE TM_{01} mode by coupling of TE_{21} and TE_{11} degenerate is shown. The field profiles are magnitudes of the overall field amplitude with E normalized to 0.1 V/m. (d)(top) Overall electric field magnitude, E and E_z field magnitude (bottom) in XZ plane at the DBE resonance of the 'butterfly' geometry and elliptical iris loaded waveguide [22]. The units are in dB (1 mV/m) [35].

Fig. 5(b). As depicted in Fig. 5(c), the degenerate TE_{11} mode coupled to the TE_{21} mode to form the DBE TM_{01}-like resonance. We remark that coupling is achieved via the mutual H_z fields supported by the TE_{11} and TE_{21} modes. It is noted that unlike DBE crystals, no bandgap was observed in dispersion diagrams. This is due to the presence of other higher order waveguide modes in the waveguide which are not affected by the geometry. One key property of the 'butterfly' geometry is its strong E_z field that leads to strong $TM_{01}-$like mode at the DBE resonance. As shown in Fig. 5(d), the strong and uniform E_z provides mode purity as compared to the elliptic iris loaded waveguide [22]. In fact, E_z field at the center ($r = 0$), is approximately 300 times stronger than that of the elliptical iris loaded waveguide as shown in Fig. 6(a). Therefore, the purity of the mode supported by the strong DBE resonance is suitable for vacuum tube devices where strong E_z field is required. The provided field profiles were obtained from CST Microwave Studio [35]. The detailed dispersion diagram for DBE mode of 'buttefly' structure was obtained via full-wave simulation using Ansoft High Frequency Simulation Software (HFSS) package, 2015 [36]. It was also verified using Computer Simulation Technology(CST) Microwave Studio [35]. It is shown in Fig. 6(b). The resonant frequency of the DBE TM_{01}-like mode is observed at approximately

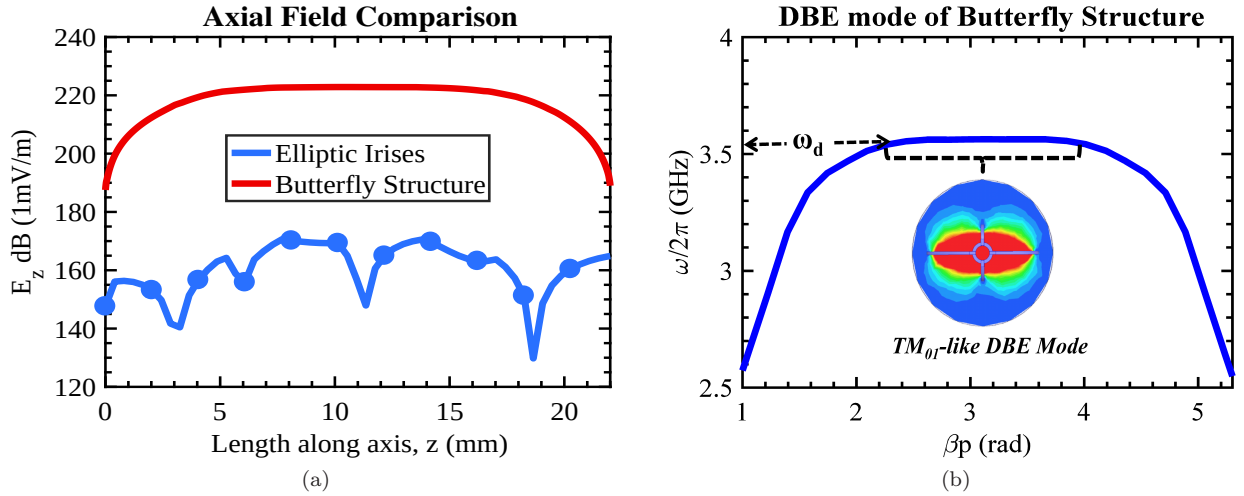

FIG. 6. (a) A comparison of E_z field along the axis of 'butterfly' geometry and elliptical iris loaded waveguide. As shown, 'butterfly' geometry provides E_z approximately 300 times larger compared to elliptic irises [22]. (b) $\omega - \beta$ diagram of 'butterfly' structure. DBE mode is depicted along with its field profile. The DBE resonance is observed at $\omega_d/2\pi = 3.52$ GHz.

$\omega_d = 3.52$ GHz.

The above geometry utilized the property of Curved Ring-bar unit cells, known for supporting TM_{01} mode. For other geometry, the mode profile defines the (L, C) parameters. The challenge is to model each mode to its transmission line equivalents and find the appropriate coupling parameters: K_{c1}, K_{c2} and K_{c3}. Hence, the above approach forms mathematical tool for all.

IV. BWO DESIGN USING 'BUTTERFLY' STRUCTURE

DBE modes have been used before to miniaturize dielectric resonator antennas by lowering their resonance frequencies [6]. They have also been demonstrated to enhance the directivity of horn antenna due to their strong resonance [38]. However, they have never been used before in high power microwave sources e.g. Traveling Wave Tubes or BWOs. These sources typically require 'mode purity' and intense axial field at the center. Previously, DBE crystals [17] or RF structures [22] supported strong resonant field. Yet, they lacked mode purity and supported hybrid modes, inapt for such applications. Since we have demonstrated that $TM_{01}-$DBE modes with mode purity can be achieved using coupled TL based 'butterfly' geometry, there is a strong potential for DBE mode based tube applications. That is, DBE mode can be useful for electron beam-RF wave interaction for vacuum tubes. However, since DBE modes are associated with narrow bandwidth, BWOs or klystrons are more appropriate applications for this. In this paper, we focus on BWO only. BWOs are active devices designed to oscillate in single frequency depending on the electron beam energy passing through it. The space charge field of the beam couple to the backwardly propagating wave, creating a feedback path for RF energy and oscillation is established. The oscillation frequency depends on the matching of the velocity of the beam and the phase velocity of the backward wave. Typically, it is the intersecting point of the beam line and $\omega - \beta$ diagram of the slow wave structure. As seen in Fig. 7(a), $\omega - \beta$ diagrams of the first 20 modes of 'butterfly' slow wave structure is given along with 52 kV beam line. The beam will interact with all modes that have E_z field at the center. To illustrate the BWO interaction with DBE mode, a BWO design was simulated using Computer Simulation Software (CST) Particle in Cell (PIC) [37] code. The BWO draws 4 A current from a circular cathode biased at 52 kV. The tube is 16 cm long and generates 68 kW power at 3.34 GHz with 33% electronic efficiency. The 'butterfly' slow wave structure is placed at the center of the waveguide as shown in Fig. 7(b). The bunching of electrons verifies the beam-wave interaction (Fig. 7(b)). Typically, the homogenous section BWOs are associated with nominal electronic efficiency of 15-20% [39, 40]. Hence, a 13-18% efficiency improvement was observed by introducing the DBE mode in the BWO using the 'butterfly' geometry.

V. CONCLUSION

We introduced a new class of TLs that can generate DbBE and DBE modes. It was demonstrated that dual pair of non-identical TLs can generate higher-order dispersion curves, specially DBE modes. Fourth-order dispersion equations were derived using the coupled mode analysis for the non-identical pair of coupled TLs. Further, it was shown that the order of the dispersion curves are dependent on the choice of coupling parameters, K_{c1}, K_{c2} and K_{c3} and dispersion can be controlled by them. An alternate approach of DBE mode realization inside circular waveguides was demonstrated via 'butterfly' ge-

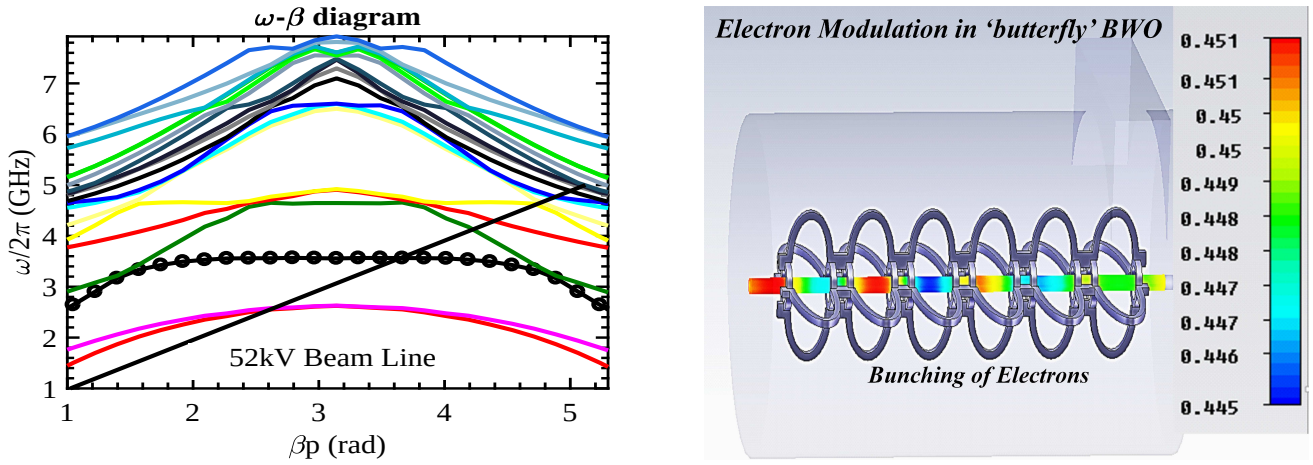

(a) (b)

FIG. 7. (a) $\omega - \beta$ diagram of the first 20 modes of 'butterfly' slow wave structure using HFSS [36]. A 52 kV, 4 A beam line is drawn to show resonant point (intersecting point of straight line and DBE mode) where beam-wave interaction takes place in a simple 'butterfly' BWO design. (b) Demonstration of beam-wave interaction in a BWO loaded with 'butterfly' slow wave structure simulated using CST PIC code [37]. The presence of bunching due to velocity modulation verifies the electron modulation process, essential for wave-particle coupling and power transfer. The color ramp shows the beam velocity, v_e normalized to the speed of light, c.

ometry, a design based on four coupled TLs. This geometry provided approximately 300 times stronger E_z field on the axis compared to elliptic irises. The presence of DBE mode verifies the coupled TLs as an effective alternative of bulk photonic crystals. The same concept can be extended further to design couplers, filters, printed circuits and to engineer new class of vacuum tubes and BWOs. An example of BWO design was presented to verify the beam-wave interaction with DBE $TM_{01}-$like mode. The BWO demonstrated efficiency improvement by 13-18% compared to nominal BWOs. This theory and example are expected to serve as tools to engineer dispersion curves for more practical applications.

ACKNOWLEDGMENTS

This research was supported by AFOSR MURI Grant FA9550-12-1-0489 administered through the University of New Mexico.

[1] E. Rajo-Iglesias, O. Quevedo-Teruel, and L. Inclan-Sanchez, IEEE Trans. Antennas Propag. **56**, 1648 (2008).
[2] N. Apaydin, L. Zhang, and J. L. Volakis, IEEE Trans. Antennas Propagat. **62**, 2954 (2014).
[3] F. Yang and Y. Rahmat-Samii, IEEE Trans. Antennas Propag. **51**, 2936 (2003).
[4] D. Sievenpiper, L. Zhang, R. F. J. Broas, N. G. Alexopolous, and E. Yablonovitch, IEEE Trans. Antennas Propag. **47**, 2059 (1999).
[5] B. Munk, *Frequency Selective Surfaces: Theory and Design* (Wiley, New York, NY, USA, 2000).
[6] G. Mumcu, K. Sertel, and J. L. Volakis, IEEE Trans. Antennas Propag. **57**, 1618 1624 (2009).
[7] C. Locker, K. Sertel, and J. L. Volakis, IEEE Microw. Wireless Compnon. Lett. **16**, 642 (2006).
[8] M. B. Stephanson, K. Sertel, and J. L. Volakis, IEEE Microw. Wireless Compon. Lett. **18**, 305 (2008).
[9] R. A. Shelby, D. R. Smith, and S. Schultz, Science **292**, 77 (2001).
[10] C. A. Balanis, *Antenna Theory: Analysis and Design* (Wiley, New York, NY, USA, 2016).
[11] D. C. Chang and C. N. Hu, Proceedings of the IEEE **100**, 2233 (2012).
[12] E. Yablonovitch, Phys. Rev. Lett. **58**, 2059 (1987).
[13] A. Figotin and I. Vitebsky, Phys. Rev. E **72-036619**, 1 (2005).
[14] A. Figotin and I. Vitebsky, Phys. Rev. A **76**, 053839 (2007).
[15] M. A. K. Othman, F. Yazdi, A. Figotin, and F. Capolino, Phys. Rev. B **93**, 024301 (2016).
[16] G. Mumcu, K. Sertel, J. L. Volakis, I. Vitebskiy, and A. Figotin, IEEE Trans. Antennas Propag. **53**, 4026 (2005).
[17] S. Yarga, K. Sertel, and J. L. Volakis, IEEE Trans. Antennas Propag. **56**, 119 (2008).
[18] N. Apaydin, L. Zhang, and J. L. Volakis, IEEE Trans. Microw. Theory Tech. **60**, 1513 (2012).
[19] A. Figotin and I. Vitebsky, Phys. Rev. E **63** (2001).
[20] A. Figotin and I. Vitebsky, Phys. Rev. B **67**, 1 (2003).
[21] J. L. Volakis and K. Sertel, in *Proceedings of IEEE*, Vol. 99 (2011) pp. 1732–1745.

[22] M. A. K. Othman and F. Capolino, IEEE Microw. Wireless Compnon. Lett. **25**, 700 (2015).
[23] M. A. K. Othman, M. Veysi, A. Figotin, and F. Capolino, Phys. Plas. **23**, 033112 (2016).
[24] S. Yarga, K. Sertel, and J. L. Volakis, IEEE Antenn. Wireless Propag. Lett. **8**, 287290 (2009).
[25] M. G. Wood, J. R. Burr, and R. M. Reano, Opt. Lett. **40**, 2493 (2015).
[26] V. A. Tamma, A. Figotin, and F. Capolino, IEEE Trans. Microw. Theory Tech. **64**, 742 (2016).
[27] S. Sensiper, in *Proceedings of IRE*, Vol. 43 (1955) pp. 149–161.
[28] D. Lopes and C. Motta, IEEE Trans. Electron Dev. **55**, 2498 (2008).
[29] M. Zuboraj and J. L. Volakis, IEEE Trans. Plas. Sci. **44**, 903 (2016).
[30] S. Liu, International Journal of Infrared and Millimeter Waves **21**, 1097 (2000).
[31] D. Watkins, *Topics in Electromagnetic Theory* (Wiley, New York, 1958).
[32] D. Marcuse, *Theory of Dielectric Optical Waveguides*, 2nd ed. (Academic Press, New York, 1991).
[33] J. Pierce, J. Appl. Phys. **25**, 179 (1954).
[34] .
[35] *CST Microwave Studio, User Manual*, Computer Simulation Technology, GmbH, Darmstadt, Germany (2016).
[36] *Ansoft HFSS 15, User Manual*, Ansys Corp., Canonsburg, PA, USA (2015).
[37] *CST Particle Studio, User Manual*, Computer Simulation Technology, GmbH, Darmstadt, Germany (2015).
[38] S. Yarga, K. Sertel, and J. L. Volakis, in *2006 IEEE Antennas and Propagation Society International Symposium* (2006) pp. 7–10.
[39] B. Levush, T. M. Antonsen, A. N. Vlasov, G. S. Nusinovich, S. M. Miller, Y. Carmel, V. L. Granatstein, W. W. Destler, A. Bromborsky, C. Schlesiger, D. K. Abe, and L. Ludeking, IEEE Trans. Plas. Sci. **24**, 843 (1996).
[40] Z. Wang, Y. Gong, Y. Wei, Z. Duan, Y. Zhang, L. Yue, H. Gong, H. Yin, Z. Lu, J. Xu, and J. Feng, IEEE Trans. Electron Dev. **60**, 471 (2013).